

Excellence in Chemistry Research

Announcing our new flagship journal

- Gold Open Access
- Publishing charges waived
- Preprints welcome
- Edited by active scientists



Meet the Editors of *ChemistryEurope*



Luisa De Cola

Università degli Studi
di Milano Statale, Italy



Ive Hermans

University of
Wisconsin-Madison, USA



Ken Tanaka

Tokyo Institute of
Technology, Japan

The Role of the Transient Atropisomerism and Chirality of Flurbiprofen Unveiled by Laser-Ablation Rotational Spectroscopy

Andrés Verde,^[a] Juan Carlos López,^[a] and Susana Blanco^{*[a]}

Abstract: The combination of atropisomerism and chirality in flurbiprofen is shown to be relevant concerning its pharmacological activity. The two most stable conformers of a total of eight theoretically predicted for each *R*- or *S*- flurbiprofen enantiomers have been isolated in the cooling conditions of a supersonic jet and structurally characterized by laser ablation Fourier transform microwave spectroscopy. The detected conformers, whose structure is mainly defined by three dihedral angles, only differ in the sign of the phenyl torsion

angle giving rise to *S_a* and *R_a* atropisomers. A comparison with the structures available for the *R*- and *S*- enantiomers complexed to COX isoforms reveals that the enzymes select only the *S_a* atropisomers, resulting in a diastereoisomer-specific recognition. The most stable gas phase conformer is exclusively selected when using the *S*- enantiomer while the second is recognized only for the *R*- enantiomer. These experimental results highlight the importance of atropisomerism in drug design.

Introduction

Non-steroidal anti-inflammatory drugs (NSAIDs) have attracted interest from the first explanation given by John Vane about the action mechanism of aspirin.^[1,2] NSAIDs inhibit non-selectively the synthesis and release of prostaglandins from arachidonic acid by the two isoforms of cyclooxygenase (COX) enzymes.^[3] One of the most commonly used NSAIDs is 2-(2-fluoro-4-biphenyl) propanoic acid, known as flurbiprofen (FB). FB is one of the most thoroughly investigated NSAIDs^[4,5] and besides its crystal structure,^[6,7] it has been observed using X-Ray diffraction forming complexes with COX enzymes,^[8–13] even at high-resolution.^[9,8] These studies show that the interaction of FB with COX at the binding pockets is the result of a complex network of polar interactions with amino acid residues including hydrogen bonds (HB), salt bridges, and even water-mediated interactions.^[11,12] FB has a stereogenic centre and as occurs for other NSAIDs^[14] its enantiomers do not exhibit the same properties.^[15] The anti-inflammatory activity is broadly stereospecific for the *S*-enantiomer, the main reason being that this enantiomer establishes a higher number of contacts with the COX active site than the *R*- form.^[8] The variety of

conformations that FB adopts upon complexation highlight the importance of the flexibility of the FB skeleton due to its torsional freedom. Related to this flexibility, it should be pointed out that the torsional motion around the single bond between the phenyl rings gives rise to transient axial chirality.^[16,17] The diastereoisomerism resulting from the combination of both the chiral centre and the labile atropisomerism could have consequences not only concerning conformation but also regarding the recognition of FB by COX.^[18]

To complete our understanding of the FB structure, a gas-phase study is needed. The inherent isolation conditions represent a perfect approximation to unveil the intrinsic properties of the molecules, their low energy conformations, and their relative energies.^[19] The most stable forms can be cooled down using supersonic jets and characterized through an appropriate spectroscopic method. Fourier transform microwave spectroscopy (FTMW) techniques provide the most precise and accurate gas phase structural data, making it possible to discriminate between conformers, like atropisomers, with minimal structural differences. Solid biomolecules with low vapour pressure and high melting point like FB are accessible by using laser ablation as a vaporization method.^[20,21] The rotational results can be fully exploited by combining them with those of theoretical calculations to explore the potential energy surface (PES) given the role of torsional flexibility in FB. For example, the height of the barrier hindering phenyl torsion is relevant since it conditions the rate of interconversion between atropisomers and their potential isolation.^[6] In this paper we have used laser ablation chirped pulse FTMW spectroscopy together with DFT B3LYP–D3BJ/6-311++G(2d,p) calculations to study FB. The two most stable atropisomers of this molecule have been isolated in the supersonic expansion. Their characterization has allowed us to show the relevance of diastereoisomerism in the recognition of FB by COX through a

[a] A. Verde, Prof. J. C. López, Prof. S. Blanco
Department of Physical Chemistry, IU CINQUIMA
Facultad de Ciencias,
Universidad de Valladolid
Paseo Belén 7, 47011 Valladolid (Spain)
E-mail: susana.blanco@uva.es

Supporting information for this article is available on the WWW under <https://doi.org/10.1002/chem.202300064>

© 2023 The Authors. Chemistry - A European Journal published by Wiley-VCH GmbH. This is an open access article under the terms of the Creative Commons Attribution Non-Commercial NoDerivs License, which permits use and distribution in any medium, provided the original work is properly cited, the use is non-commercial and no modifications or adaptations are made.

global analysis of the results obtained in this work for the bare FB and those reported for the COX-FB complexes.

Results and Discussion

FB may adopt several conformations thanks to the rotation around single bonds. The dihedral angles α ($C_1-C_6-C_7-C_{12}$), β ($C_9-C_{10}-C_{14}-C_{15}$) and γ ($C_{10}-C_{14}-C_{16}-O_{17}$) (see Figures S1 and S2) are coordinates appropriate to define these internal rotations. α describes the rotation of the phenyl ring, β the rotation of the propanoic group and γ the rotation of the carboxylic group. Relaxed scans along these coordinates show the existence of 8 different conformers for each enantiomer. The conformers found are depicted in Figure 1 for the *S*-enantiomer and the relevant spectroscopic parameters are given in Table S1. The full set of conformers including those for the *R*-enantiomer are shown in Figures S3 and S4. Besides the identification of the *S*- or *R*-enantiomers, to label the conformers we have considered first the configuration of the propanoic acid relative to the *o*-fluorophenyl group (see Figure S2). The four possible config-

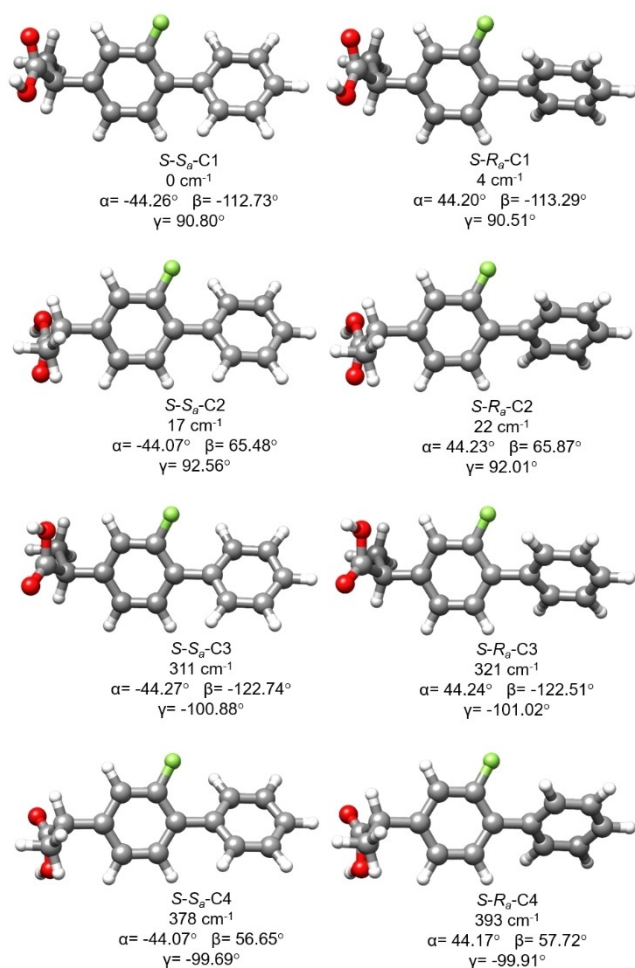


Figure 1. Predicted conformers of *S*-FB. Relative energies and dihedral angles were calculated at B3LYP–D3BJ/6-311++G(2d,p) level. See also Figures S3 and S4.

urations have been named C1–C4 in order of increasing relative energy. Furthermore, for each of these arrangements, phenyl group rotation gives rise to *S_a* and *R_a* atropisomers, according to axial chirality nomenclature conventions.

The chirped pulse FTMW jet-cooled rotational spectrum of laser-ablated FB is given in Figure S5. The excerpt in Figure 2 shows the identification of two rotamers, labelled *i* and *ii*, both with dominant *b*-type spectra. The assignment of the spectrum is detailed in the Experimental Section. The spectra were analysed using the *S*-reduced semirigid rotor Hamiltonian of Watson^[22] set up in the *I'* representation. The experimental rotational parameters are collected in Table 1 and the observed frequencies are given in Tables S8 and S9.

The experimental rotational constants, nearly equal for both rotamers, are quite close to those predicted for the conformers of C1 and C3 families (see Tables 1 and S1). However, the observation of dominant *b*-type spectra rules out the C3 family, having low values of the μ_b electric dipole moment component. Finally, comparing the trends in the variation of the rotational constants and planar moments of inertia between the observed rotamers and the C1 atropisomers, rotamers *i* and *ii* could then be assigned to the conformers *S*-*S_a*-C1 and *S*-*R_a*-C1, respectively, or their specular images *R*-*R_a*-C1 and *R*-*S_a*-C1, respectively, taking into account that a racemic mixture has been used.

The potential energy function describing the phenyl torsion which interconverts the detected forms shown in Figure 3 is similar to that of *o*-fluorobiphenyl (see Figure S18). It presents two equivalent barriers at the coplanar rings configuration ($\alpha = 0^\circ, 180^\circ$; $B_0 = 1016 \text{ cm}^{-1}$) and two equivalent barriers at the perpendicular rings configuration ($\alpha = 90^\circ, -90^\circ$; $B_{90} = 562 \text{ cm}^{-1}$). However, differently with *o*-fluorobiphenyl having four equivalent minima, FB shows two equivalent minima at *S*-*S_a*-C1 form (-44.3° and 135.7°) and two different equivalent minima at *S*-*R_a*-C1 configuration (-135.8° and 44.2°), predicted at B3LYP–D3BJ/6-311++G(2d,p) level only 4 cm^{-1} above the *S*-*S_a*-C1 form. Considering the collisional relaxation processes taking place in the supersonic jet and the use of Ar as the carrier gas,^[23] the observation of both rotamers is consistent with the existence of potential barriers higher than 400 cm^{-1}

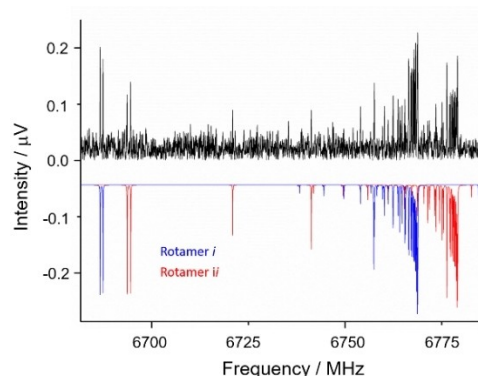


Figure 2. A 6.6–6.9 GHz section of the CP-FTMW spectrum of laser-ablated FB. The spectra calculated from the experimentally determined rotational parameters are shown below, in blue for rotamer *i* and in red for rotamer *ii*.

Table 1. The experimental rotational parameters for the observed rotamers of flurbiprofen are compared to those predicted at B3LYP–D3BJ/6-311++G(2d,p) level for the most stable conformers and those calculated from the fitted structures.

Param. ^[a]	Rotamer <i>i</i>	<i>S-S_σ</i> -C1 DFT	<i>S-S_σ</i> -C1 fitted structure	Rotamer <i>ii</i>	<i>S-R_σ</i> -C1 DFT	<i>S-R_σ</i> -C1 fitted structure
<i>A</i> /MHz	1152.19764(30) ^[b]	1153.8	1152.2	1153.63996(37)	1154.7	1153.6
<i>B</i> /MHz	189.19205(12)	189.2	189.6	189.52867(11)	189.4	189.8
<i>C</i> /MHz	181.23098(11)	180.8	181.3	180.83555(11)	180.5	180.9
<i>D_j</i> /kHz	0.00201(22)			0.00271(22)		
<i>D_{JK}</i> /kHz	0.0326(21)			0.0132(26)		
<i>κ</i>	−0.98	−0.98	−0.98	−0.98	−0.98	−0.98
<i>P_{aa}</i> /uÅ ²	2510.6092(18)	2514.2	2507.2	2511.5601(17)	2514.8	2509.9
<i>P_{bb}</i> /uÅ ²	277.9819(18)	281.0	280.3	283.1288(17)	284.5	285.3
<i>P_{cc}</i> /uÅ ²	160.6400(18)	157.0	158.3	154.9447(17)	153.2	152.8
<i>n</i>	93			82		
<i>σ</i> /kHz	7.5			7.7		

[a] *A*, *B* and *C* are the rotational constants. *κ* is the Ray asymmetry parameter. *D_j* and *D_{JK}* are the quartic centrifugal distortion constants. $\kappa = (2B - A - C)/(A - C)$. *P_{αα}* (*α* = a, b, c) are the planar moments of inertia, derived from the inertial moments $P_{cc} = (I_a + I_b - I_c)/2$. *n* is the number of fitted lines. *σ* is the rms deviation of the fit. [b] Standard errors in parenthesis in units of the last digit.

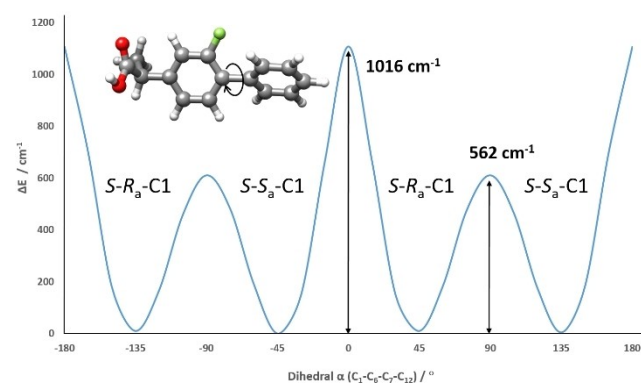


Figure 3. Calculated B3LYP–D3BJ/6-311++G(2d,p) potential energy function of S-FB as a function of the dihedral angle α ($C_1-C_6-C_7-C_{12}$) defining the phenyl group torsion. The potential energy function calculated for the *R*-enantiomer is a specular image of this one (Figure S6). See also Figures S7–S9 describing this potential function for other conformers.

between them, quenching the possible relaxation of the less stable atropisomer *S-R_σ*-C1 to the global minimum *S-S_σ*-C1 form. According to Figure 3, the interconversion between the observed atropisomers would occur preferentially through the barrier at the orthogonal-rings configuration. The value of this barrier characterizes this atropisomerism as belonging to class 1.^[24]

The non-observation of conformers C2 with an energy similar to that of C1 forms can be attributed to their low dipole moment components (see Table S1). The barriers calculated for the interconversion between C3 and C1 forms and between C4 and C2 families make conformers C3 and C4 susceptible to suffer a collisional relaxation in the supersonic jet to forms C1 and C2 respectively (see Figures S10–S17).

DFT structures can be taken as a good description of the geometries of the observed forms based on the agreement between experimental and theoretical rotational constants. However, since biomolecules are very flexible systems, it is reasonable to fit the torsional angles to obtain a structure that better reproduces the rotational parameters. Assuming the DFT structure and keeping the phenyl rings planar, we have

analysed the dependence of the rotational constants on the torsional angles. Variations of the α and γ angles do not induce significant changes in the values of the rotational constants. However, small changes in β almost bring the rotational constants to the experimental values. In this way, fits of the rotational constants gave values of $\beta = -114.9(2)^\circ$ for *S-S_σ*-C1 and $\beta = -114.3(1)^\circ$ for *S-R_σ*-C1 conformers. The rotational constants calculated from these structures are shown in Table 1 where they can be compared with the experimental ones.

Essentially, the distinctive structural difference between both detected conformers is the orientation of the phenyl ring, shown by the opposite sign of the α angle values (see Figure 4). The corresponding values are quite similar to that of $\pm 44.4(1.2)^\circ$ determined for the biphenyl molecule in gas-phase.^[25] For fluorobiphenyl, it has been determined as $\pm 54.1^\circ$ in condensed phases using X-ray techniques^[26] and $\pm 49(5)^\circ$ by gas-phase electron diffraction.^[27] The balance of forces yielding almost the same torsional angle between the phenyl planes in FB, biphenyl, and *o*-fluorobiphenyl involves the π -conjugation between the two rings favouring a co-planar configuration and the steric repulsion between the adjacent atoms in *ortho*-position.

Quantum Theory of “atoms in molecules” (QTAIM)^[28,29] and non-covalent interaction (NCI)^[30] analyses were done to better understand other possible interactions stabilising the FB

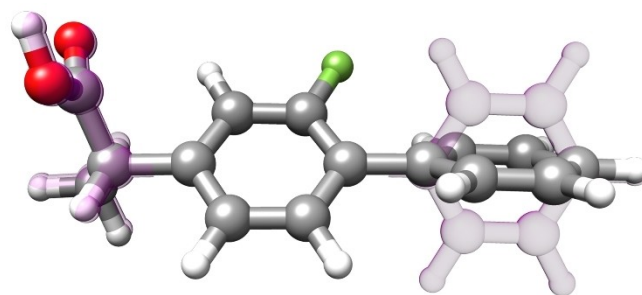


Figure 4. Comparison between the *S-S_σ*-C1 (in grey) and *S-R_σ*-C1 (in purple) FB experimental structures.

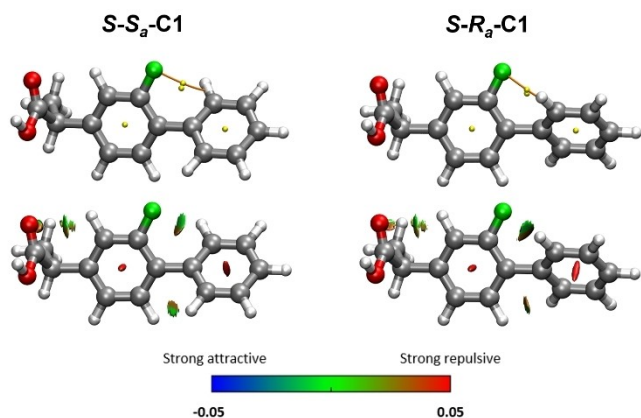


Figure 5. The QTAIM analysis plot shows critical points in yellow and bond paths in orange. NCI plots map the location and strength of intramolecular interactions with coloured isosurfaces ranging from blue (attractive) to red (repulsive) according to the product of the sign of the second eigenvalue of the Hessian and electron density, $\text{sign}[\lambda_2(r)]\rho(r)$.

conformations. The results, shown in Figure 5 indicate the presence of a weak CH...F intramolecular HB between the polar fluorine atom and the closest hydrogen atom in the other phenyl ring that stabilizes the observed structures. The CH...F distance is 2.482 Å in *S-S_a-C1* and 2.479 Å in *S-R_a-C1*. In addition, taking into account that the electronic density ($\rho(r)$) is related to the strength of the bond^[31,32] the interaction energies are estimated to be $-1.56 \text{ kcal mol}^{-1}$ for *S-S_a-C1* and $-1.57 \text{ kcal mol}^{-1}$ for *S-R_a-C1*. These weak HBs can be gathered from the bond paths and the (3,-1) bond critical points resulting from the QTAIM analysis. There is a (3,+1) ring critical point of cyclic structures that shows the HB closing a *pseudo* six-membered ring ($\text{C}_1\text{-C}_6\text{-C}_7\text{-C}_{12}\text{-H}_{19}\text{-F}_{13}$). NCI shows additional weak attractive interactions for example the CH...O contact between the carbonyl oxygen atom and one methyl group hydrogen atom. The corresponding H...O distances are 2.685 Å for *S-S_a-C1* and 2.686 Å for *S-R_a-C1*. There is another weak interaction between the carbonyl oxygen and the closest hydrogen of the ring with distances of 2.685 Å for *S-S_a-C1* and 2.693 Å for *S-R_a-C1*. Weak repulsive interactions can be also observed.

We have compared the structures of the gas-phase observed and predicted conformations (Tables S2 and S3) with those found in condensed phases for the pure *S*-FB enantiomer (Table S4), for the complexes of COX with *S*-FB (COX-1 in Table S5 and COX-2 in Table S6), and those for the complexes

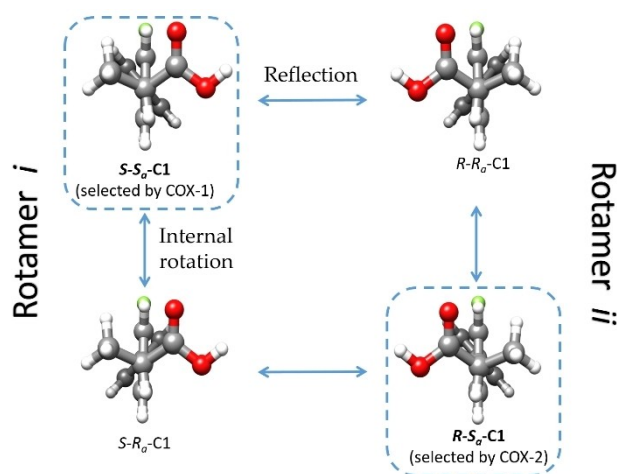


Figure 6. Selective recognition of FB gas phase conformers by COX.

with *R*-FB (COX-2 Table S7). The X-Ray diffraction dihedral angle values for crystalline *S*-FB^[6,7] show the detection of structures close to *S-S_a-C1* and *S-S_a-C4*. *S*-FB interacting with COX-1^[9,11,12] has been detected in conformations identifiable as *S-S_a-C1*, *S-S_a-C2*, and *S-S_a-C4*. When *S*-FB is complexed to COX-2,^[13] *S-S_a-C2* is selected. On the other hand, the *R*-enantiomer linked to COX-2^[8] shows structures related to *R-S_a-C1* or *R-S_a-C3*. In all the cases, we have established the relation between condensed phase structures and gas phase forms by identifying the conformer to which DFT geometry optimizations of the condensed phase forms converge. In Table 2 the gas phase structures of C1 forms are compared with those detected using high-resolution X-Ray diffraction for *S*-FB and *R*-FB recognized by COX-1 and COX-2 respectively.^[9,8] It should be highlighted that only the *S_a* axial chirality arrangement is recognized by COX isoforms independently of the FB enantiomer. Due to this, if we consider the conformers detected in the gas phase in this work, COX enzymes select exclusively *S-S_a-C1* for the *S*-enantiomer and *R-S_a-C1* for the *R*-enantiomer as can be inferred from Figure 6. This *S_a* selectivity of COX isoforms is possible given the transient or labile character of the atropisomerism of 2-fluorobiphenyl moiety.

Table 2. Comparison of angles between gas-phase conformers and high resolution X-Ray data on FB-COX complexes.

Param. ^[a]	<i>S-R_a-C1</i>	<i>S-S_a-C1</i>	<i>S</i> -FB-COX-1 ^[9]	<i>R-R_a-C1</i> ^[c]	<i>R-S_a-C1</i> ^[c]	<i>R</i> -FB-COX-2 ^[8]
α ($\text{C}_1\text{-C}_6\text{-C}_7\text{-C}_{12}$)/°	44.2	-44.3	-48.6	44.3	-44.2	-40.8
β ($\text{C}_9\text{-C}_{10}\text{-C}_{14}\text{-C}_{13}$)/°	-114.3(1)	-114.9(2)	-142.9	114.9(2) ^[b]	114.3(1)	101.2
γ ($\text{C}_{10}\text{-C}_{14}\text{-C}_{16}\text{-O}_{17}$)/°	90.5	90.8	78.9	-90.8	-90.5	-74.4/108.8

[a] See Figure S1 for notation. α and γ angle values for C1 forms are taken from DFT structures and β from the fitted structures. [b] Standard errors in parenthesis in units of the last digit. [c] *R-R_a-C1*, *R-S_a-C1* parameters were obtained based on their mirror imaged relationship to *S-S_a-C1*, *S-R_a-C1*, respectively.

Conclusion

In this work, the rotational spectrum of FB has been observed for the first time. The spectra of two rotamers showing similar intensities and close rotational parameters have been assigned. These rotamers have been identified as the two most stable conformers out of a total of eight low-energy conformers predicted theoretically, sixteen if we take into account the chiral nature of FB. The observed forms S - S_a -C1/ R - R_a -C1 and S - R_a -C1/ R - S_a -C1 correspond to the two possible atropisomers arising from the axial chirality of 2-fluorobiphenyl moiety, differing mainly on the orientation of the phenyl end group with torsional dihedral angles of approximately -44° and $+44^\circ$. The experimental isolation and characterization of these conformers has been possible using laser ablation combined with a supersonic expansion. The FB sample has been vaporized by laser ablation and seeded into a supersonic expansion, where the cooling conditions allow the isolation of the two most stable conformers in their ground vibrational states in gas phase. The experimental detection of both conformers has been carried out by FTMW spectroscopy, one of the most definitive structural probes.

By comparing the structures of the isolated forms with those detected by X-Ray diffraction for FB interacting with COX isoforms we can conclude that the configurations adopted by FB upon complexation are accessible from the isolated FB conformers with low energy cost. The interplay between the chiral centre and the axial chirality in FB has important consequences in the interaction with the enzyme: i) COX chiral recognition of FB is not only different concerning the R - or S -enantiomers derived from the existence of a chiral centre but also with respect to the axial chirality associated to the fluorobiphenyl group. COX enzymes select exclusively the S_a atropisomers independently of the interacting enantiomer. This selectivity is possible due to the low $S_a \leftrightarrow R_a$ interconversion barrier leading to a transient or labile atropisomerism. ii) This behaviour leads to the outstanding fact that only one of the two forms cooled in the supersonic jet is recognized in the interaction of S -FB with COX while the other is observed only for the interaction with the R - enantiomer. The gas phase study shows the most stable conformers in their ground vibrational state, free of the intermolecular interactions present in condensed phases. As deduced from the structures observed for FB in the complexes with COX-1 and COX-2, interactions with the enzyme limit the accessible configurations to S_a arrangement of the rings. Nevertheless, a more detailed study of the intermolecular interactions and steric limiting factors in the COX pockets would allow to better understand the role of interactions within the receptor. The obtained results highlight the role that atropisomerism can play in drug design and the challenges it poses.^[18]

Experimental Section

Microwave experiment: The experiment was conducted on a chirped-pulse Fourier transform microwave spectrometer (2-8 GHz)

incorporating a Q-switch Nd/YAG laser ablation source.^[21,33] A solid bar of the sample was prepared by compressing a 1:1 mixture of the grinded flurbiprofen (FB) commercial sample (m.p. 110–111 °C; b.p. 162.4 °C) and Cu powder. This rod was held in a special laser ablation nozzle adapted from previous designs.^[34,35] To vaporize the sample, the laser was focused on the surface of the rod, which was continuously translated and rotated to improve the reproducibility of the ablation process. Once the sample was vaporized it was dragged by the carrier gas (Argon, 6 bar stagnation pressure) expanding into the vacuum chamber as a supersonic jet. There, the molecules were excited using a 4 μ s pulsed microwave chirp generated by an arbitrary waveform generator and amplified (200 W) by a TWT amplifier. This chirp pulse covered the whole 2–8 GHz range and was emitted by a microwave horn antenna. The free induction decay (FID) emitted after polarization was detected through a second horn, recorded in the time domain with a digital oscilloscope and Fourier transformed to the frequency domain. The polarization-detection cycle was repeated up to eight times per molecular expansion pulse, obtaining a total of eight averaged spectra in every molecular jet pulse. The repetition rate of molecular pulses was 5 Hz allowing optimal vacuum conditions in the chamber. The spectrum recorded is the result of the accumulation of 1 million spectra. The accuracy of frequency measurements is estimated to be better than 15 kHz.

Rotational spectra: All conformers of FB are prolate asymmetric rotors with very low values of μ_a (Table S1). Some of them present moderate values of μ_b and/or μ_c . The chirped pulse FTMW jet-cooled rotational spectrum of laser-ablated FB recorded in the 2–8 GHz region shows very weak lines (see Figures 2 and S5). Initial trials to assign the spectra of FB were done with the rotational constants of the most stable conformer. The assignment of two sets of b -type R-branch rotational lines led to the identification of two rotamers, initially labelled i and ii , both with similar rotational constants. A careful analysis allowed the assignment of a few c -type lines for rotamer ii . The internal rotation of the methyl group does not generate detectable A–E splittings. Unfortunately, it was not possible to observe ^{13}C monosubstituted isotopologues in natural abundance due to the low signal-to-noise ratio observed.

Flexible model computations^[36] to investigate the phenyl torsion potential energy function from the observed rotational parameters show that the observed constants are not very sensitive to changes in the PES parameters. Nevertheless, calculations from a simple model approximately predict the rotational constants and planar moment observed trends, thus confirming the assignment.

Another experimental fact is the observed intensity ratio for the μ_b -type transitions indicating that rotamer i is slightly more intense than rotamer ii ($I_i/I_{ii} = 1.3(0.1)/1$). The value of the ratio predicted for the squared μ_b dipole moment ($2.44\text{D}^2/2.38\text{D}^2 = 1.06$) confirms the assignment taking into account three times the standard error. In addition, the proportionality of the observed intensities to $N_j \cdot \mu_j^2$, where N_j is the number density of species j in the supersonic jet and μ_j is the value of the dipole moment component, indicates an almost equal population of both rotamers in the supersonic jet.

Computational: The conformational study of FB was done with the help of CREST^[37] (conformer-rotamer ensemble sampling tool) and following chemical intuition to complete the conformational search by exploring the potential energy surface (PES). The geometries of all the conformers were optimized using the B3LYP hybrid functional,^[38] B3LYP–D3 using Grimme's empirical dispersion correction (D3)^[39] and B3LYP–D3BJ corresponding to the Becke and Johnson damping factor (D3BJ).^[40,41] In all cases Pople's 6–311++G(2d,p) basis set^[42] were used employing GAUSSIAN16^[43] package. Further calculations of the vibrational frequencies were carried out within the harmonic approximation to verify that the obtained

conformers were indeed minima in the PES. The geometries obtained from the three methods are very similar for each conformer with the same trends for the rotational constants, planar inertial moments, and the relative energies (Table S1). In addition, the energies predicted for the transition conformers are quite similar. Since it is expected that the use of the dispersion terms will lead to better values of the interconversion barriers, we have used the B3LYP–D3BJ results for further discussions. It can be observed that the Becke and Johnson corrections predict slightly lower interconversion barriers, although high enough to avoid the conformational relaxation in the supersonic expansion.

Quantum theory of “atoms in molecules” (QTAIM)^[28] and non-covalent interaction (NCI)^[30] analyses were done using the Multiwfn program^[29] with the B3LYP–D3BJ/6-311++G(2d,p) results to obtain complementary information about the nature of the intramolecular interactions that stabilize the observed conformers.

Acknowledgements

The authors acknowledge the Junta de Castilla y León (Grant INFRARED-FEDER IR2020-1-UVa02), the Ministerio de Economía y Competitividad (Grant CTQ2016-75253-P) and the Ministerio de Ciencia e Innovación (Grant PID2021-125207NB–C33).

Conflict of Interest

The authors declare no conflict of interest.

Data Availability Statement

The data that support the findings of this study are available in the supplementary material of this article.

Keywords: atropisomerism · chirality · flurbiprofen · laser ablation · rotational spectroscopy

- [1] J. R. Vane, *Nat. New Biol.* **1971**, *231*, 232–235.
- [2] J. R. Vane, *J. Physiol. Pharmacol.* **2000**, *51*.
- [3] J. K. Gierse, S. D. Hauser, D. P. Creely, C. Koboldt, S. H. Rangwala, P. C. Isakson, K. Seibert, *Biochem. J.* **1995**, *305*, 479–484.
- [4] C. A. Rouzer, L. J. Marnett, *Chem. Rev.* **2020**, *120*, 7592–7641.
- [5] M. E. Di Pietro, C. Aroulanda, G. Celebre, D. Merlet, G. De Luca, *New J. Chem.* **2015**, *39*, 9086–9097.
- [6] K. Manoj, H. Takahashi, T. Hirohito, R. Tamura, *Experimental Crystal Structure Determination* **2016**, *CCDC 931855*, 10.5517/ccdc.csd.cc108nvs.
- [7] J. L. Flippen, R. D. Gilardi, *Acta Crystallogr. Sect. B* **1975**, *31*, 926–928.
- [8] K. C. Duggan, D. J. Hermanson, J. Musee, J. J. Prusakiewicz, J. L. Scheib, B. D. Carter, S. Banerjee, J. A. Oates, L. J. Marnett, *Nat. Chem. Biol.* **2011**, *7*, 803–809.
- [9] K. Gupta, B. S. Selinsky, P. J. Loll, *Acta Crystallogr. Sect. D* **2006**, *62*, 151–156.
- [10] D. Picot, R. M. Garavito, *Nature* **1994**, *367*, 7.
- [11] B. S. Selinsky, K. Gupta, C. T. Sharkey, P. J. Loll, *Biochemistry* **2001**, *40*, 5172–5180.
- [12] R. S. Sidhu, J. Y. Lee, C. Yuan, W. L. Smith, *Biochemistry* **2010**, *49*, 7069–7079.
- [13] R. G. Kurumbail, A. M. Stevens, J. K. Gierse, J. J. McDonald, R. A. Stegeman, J. Y. Pak, D. Gildehaus, J. M. iyashiro, T. D. Penning, K. Seibert, P. C. Isakson, W. C. Stallings, *Nature* **1996**, *384*, 644–648.
- [14] S. S. Adams, P. Bresloff, C. G. Mason, *J. Pharm. Pharmacol.* **1976**, *28*, 256–257.
- [15] N. M. Davies, *Clin. Pharmacokinet.* **1995**, *28*, 100–114.
- [16] F. Leroux, *ChemBioChem* **2004**, *5*, 644–649.
- [17] I. Alkorta, J. Elguero, C. Roussel, N. Vanthuyne, P. Piras, in *Advances in Heterocyclic Chemistry* (Ed.: A. Katritzky), Academic Press, **2012**, pp. 1–188.
- [18] J. Clayden, W. J. Moran, P. J. Edwards, S. R. LaPlante, *Angew. Chem. Int. Ed.* **2009**, *48*, 6398–6401; *Angew. Chem.* **2009**, *121*, 6516–6520.
- [19] J. L. Alonso, J. C. López, in *Gas-Phase IR Spectroscopy and Structure of Biological Molecules* (Eds.: A. M. Rijs, J. Oomens), Springer International Publishing, Cham, **2014**, pp. 335–401.
- [20] S. Blanco, A. Macario, J. C. López, *Phys. Chem. Chem. Phys.* **2021**, *23*, 13705–13713.
- [21] J. C. López, A. Macario, A. Verde, A. Pérez-Encabo, S. Blanco, *Molecules* **2021**, *26*, 7585.
- [22] J. K. G. Watson, *Vibrational Spectra and Structure: A Series of Advances. Vol. 6*, Elsevier, Amsterdam, **1977**.
- [23] R. S. Ruoff, T. D. Klots, T. Emilsson, H. S. Gutowsky, *J. Chem. Phys.* **1990**, *93*, 3142–3150.
- [24] S. T. Toenjes, J. L. Gustafson, *Future Med. Chem.* **2018**, *10*, 409–422.
- [25] A. Almendinger, O. Bastiansen, L. Fernholt, B. N. Cyvin, S. J. Cyvin, S. Samdal, *J. Mol. Struct.* **1985**, *128*, 59–76.
- [26] Rajnikant, D. Watkin, G. Tranter, *Acta Crystallogr. Sect. C* **1995**, *51*, 1452–1454.
- [27] O. Bastiansen, L. Smedvik, *Acta Chem. Scand.* **1954**, *8*, 1593–1598.
- [28] R. F. W. Bader, *Chem. Rev.* **1991**, *91*, 893–928.
- [29] T. Lu, F. Chen, *J. Comput. Chem.* **2012**, *33*, 580–592.
- [30] E. R. Johnson, S. Keinan, P. Mori-Sánchez, J. Contreras-García, A. J. Cohen, W. Yang, *J. Am. Chem. Soc.* **2010**, *132*, 6498–6506.
- [31] G. Salvitti, S. Blanco, J. C. López, S. Melandri, L. Evangelisti, A. Maris, *J. Chem. Phys.* **2022**, *157*, 144303.
- [32] S. Emamian, T. Lu, H. Kruse, H. Emamian, *J. Comput. Chem.* **2019**, *40*, 2868–2881.
- [33] S. Blanco, A. Macario, J. C. López, *Phys. Chem. Chem. Phys.* **2021**, *23*, 13705–13713.
- [34] R. D. Suenram, F. J. Lovas, G. T. Fraser, K. Matsumura, *J. Chem. Phys.* **1990**, *92*, 4724–4733.
- [35] K. A. Walker, M. C. L. Gerry, *J. Mol. Spectrosc.* **1997**, *182*, 178–183.
- [36] R. Meyer, *J. Mol. Spectrosc.* **1979**, *76*, 266–300.
- [37] P. Pracht, F. Bohle, S. Grimme, *Phys. Chem. Chem. Phys.* **2020**, *22*, 7169–7192.
- [38] C. Lee, W. Yang, R. G. Parr, *Phys. Rev. B* **1988**, *37*, 785–789.
- [39] S. Grimme, J. Antony, S. Ehrlich, H. Krieg, *J. Chem. Phys.* **2010**, *132*, 154104.
- [40] E. R. Johnson, A. D. Becke, *J. Chem. Phys.* **2006**, *124*, 174104.
- [41] S. Grimme, S. Ehrlich, L. Goerigk, *J. Comput. Chem.* **2011**, *32*, 1456–1465.
- [42] R. Ditchfield, W. J. Hehre, J. A. Pople, *J. Chem. Phys.* **1971**, *54*, 724–728.
- [43] M. J. Frisch, G. W. Trucks, H. B. Schlegel, G. E. Scuseria, M. A. Robb, J. R. Cheeseman, G. Scalmani, V. Barone, G. A. Petersson, H. Nakatsuji, X. Li, M. Caricato, A. V. Marenich, J. Bloino, B. G. Janesko, R. Gomperts, B. Mennucci, H. P. Hratchian, J. V. Ortiz, A. F. Izmaylov, J. L. Sonnenberg, D. Williams-Young, F. Ding, F. Lipparini, F. Egidi, J. Goings, B. Peng, A. Petrone, T. Henderson, D. Ranasinghe, V. G. Zakrzewski, J. Gao, N. Rega, G. Zheng, W. Liang, M. Hada, M. Ehara, K. Toyota, R. Fukuda, J. Hasegawa, M. Ishida, T. Nakajima, Y. Honda, O. Kitao, H. Nakai, T. Vreven, K. Throssell, J. A. Montgomery, Jr., J. E. Peralta, F. Ogliaro, M. J. Bearpark, J. J. Heyd, E. N. Brothers, K. N. Kudin, V. N. Staroverov, T. A. Keith, R. Kobayashi, J. Normand, K. Raghavachari, A. P. Rendell, J. C. Burant, S. S. Iyengar, J. Tomasi, M. Cossi, J. M. Millam, M. Klene, C. Adamo, R. Cammi, J. W. Ochterski, R. L. Martin, K. Morokuma, O. Farkas, J. B. Foresman, D. J. Fox, *Gaussian 16 Revision A.01*, Gaussian Inc. Wallingford CT **2016**.
- [44] M. J. Frisch, et al., *Gaussian 16 Revision A.01*, Gaussian Inc. Wallingford CT **2016**.

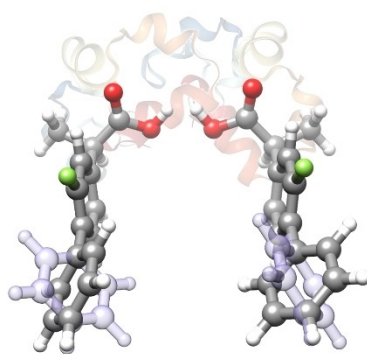
Manuscript received: January 9, 2023

Accepted manuscript online: February 24, 2023

Version of record online: ■■■■■

RESEARCH ARTICLE

The two most stable conformers of flurbiprofen (FB) have been isolated. They only differ in the dihedral angle that defines the arrangement of the phenyl group revealing FB atropisomerism. Analysing the recognition of FB by COX isoforms, it comes out that only one of these atropisomers is specifically selected for each *R*- or *S*-enantiomer.



A. Verde, Prof. J. C. López, Prof. S. Blanco*

1 – 7

The Role of the Transient Atropisomerism and Chirality of Flurbiprofen Unveiled by Laser-Ablation Rotational Spectroscopy

